

RESEARCH ARTICLE

Design and Analysis of Hybrid-Excitation Variable Flux Memory Motor for Traction Applications: Improving Output Power in High-Speed Area During Six-Step Operation Mode

REN TSUNATA¹, (Member, IEEE), KEITO YOKOMICHI,
MASATSUGU TAKEMOTO¹, (Member, IEEE), AND JUN IMAI, (Member, IEEE)

Graduate School of Environmental, Life, Natural Science and Technology, Okayama University, Kita-ku, Okayama 700-8530, Japan

Corresponding author: Ren Tsunata (tsunata@okayama-u.ac.jp)

ABSTRACT Variable flux motors with adjustable magnetic flux have been gaining attention because of their capability to simultaneously achieve a high torque density and high efficiency. In addition, the output power characteristic, which is related to acceleration performance, in high-speed areas is important in traction applications. However, typical traction motors have lower output power in high-speed areas. In this paper, a Hybrid-Excitation Variable Flux Memory Motor (HE-VFMM) is therefore proposed to enhance output power characteristics under six-step operation mode in high-speed area. The proposed HE-VFMM can perform magnetic flux adjustment with two components: field winding and variable flux permanent magnet (VPM), thus dramatically increasing flux adjustment range. The simulation results show the proposed HE-VFMM achieves 23.7% higher output power at 17,000 rpm than that of an existing traction motor in Prius 4th generation that has the same size while maintaining high efficiency in the frequently used operating area. Additionally, it was found that variable magnetic flux is very effective in enhancing the output power, especially in the high-speed region because the magnetic saturation in the stator core is mitigated by field-weakening control. Consequently, as the rotational speed increases, an increase ratio of the output power caused by the adjustable magnetic flux becomes higher. This paper shows that the proposed HE-VFMM is an effective method for improving the problem of low output power in high-speed regions in traction motors.

INDEX TERMS Variable flux memory motor, hybrid excitation motor, traction applications, EV, HEV, six-step operation, one-pulse drive, output power density.

I. INTRODUCTION

Traction motors for EV and HEV require high torque density and efficiency [1]. In addition, the output power characteristic in high-speed areas is also important in traction applications because it is related to acceleration performance. However, as shown in Fig. 1 typical traction motors are prone to have a lower output power in the high-speed area than its peak point around the base speed [2], [3]. Accordingly, to improve the acceleration performance in high-speed areas, it is essential to increase the motor size. On the other hand,

if the output power in the high-speed area is increased with a fixed motor size, the efficiency in the frequently used operating area decreases. Thus, this paper aims to address the problem of low output power in the high-speed area of traction motors while maintaining motor size and high efficiency.

In recent years, variable flux motors with adjustable flux leakage have been gaining attention because they can achieve high torque density and efficiency. With variable flux motors, the magnetic flux can be properly adjusted, so there is a possibility of improving the output power in high-speed areas while maintaining the same motor size and high-efficiency performance. Variable flux motors can be classified into

The associate editor coordinating the review of this manuscript and approving it for publication was Amin Mahmoudi¹.

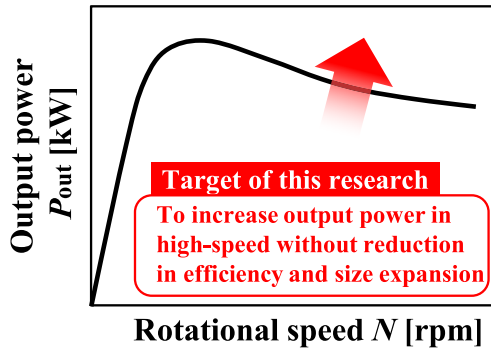


FIGURE 1. Typical characteristic of output power of traction motors and goal of this research.

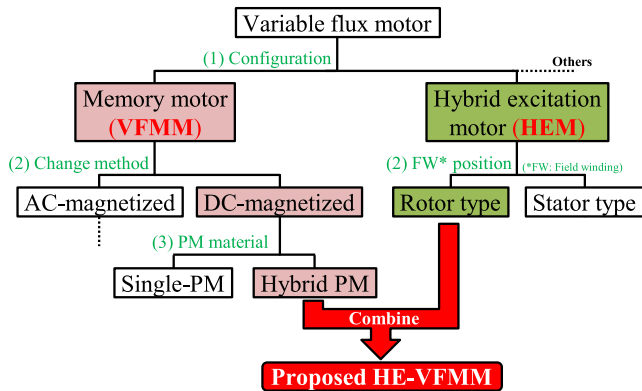


FIGURE 2. Classification of typical variable flux motors and position of proposed HE-VFMM.

various configuration. Fig. 2 shows classification of typical variable flux motors and position of the proposed motor in this research. One of the typical configurations is Variable flux memory motor (VFMM). VFMM can change the magnetization state of permanent magnet (PM) by pulse current. Additionally, VFMMs are classified into AC-magnetized and DC-magnetized type by the magnetization method [4], [5]. Furthermore, each type can be classified into single-PC and hybrid-PM types, and various structures are being studied [6], [7]. In recent years, the hybrid-PM type has been actively investigated because its high output density and high variable magnetic field capacity.

On the other hand, there is a structure such as a hybrid excitation motor (HEM) that has variable field magnetism using PM and field winding (FW) [8]. HEMs can be classified according to whether the FW is installed in the rotor or stator. A slip ring is required to apply the field current to the FW on the rotor, but high field adjustment capability can be achieved. On the other hand, when the FW is installed in the stator, a slip ring is not necessary, but the variable flux range is reduced.

Our research group has proposed hybrid-excitation variable flux memory motor (HE-VFMM), which achieves greater performance by combining VFMM and HEM [9]. The proposed HE-VFMM can perform magnetic flux adjustment with two components: the field winding and variable flux

permanent magnets (VPM), thus dramatically increasing flux adjustment range. As a result, the proposed HE-VFMM is likely to realize much higher efficiency and output power simultaneously compared with typical interior permanent magnet synchronous motors (IPMSM) with constant magnetic flux.

The efficiency of the proposed HE-VFMM has already been investigated, and its performance is superior to a traction motor in the Toyota Prius 4th generation [9]. In this paper, the output power performance of the proposed HE-VFMM was investigated and compared to that of the traction motor in the Prius 4th generation as a target motor. Their output power is evaluated under the six-step operation mode because the target motor operates with this control method in the high-speed region. The simulation results show that the proposed HE-VFMM achieves 23.7% higher output power at 17,000 rpm than that of the target motor. This result shows that the proposed HE-VFMM can dramatically enhance the acceleration characteristics in the high-speed region, which is one of the drawbacks of traction motors. In addition, this paper proposes and evaluates a non-constant air gap for the HE-VFMM to enhance the efficiency in the six-step operation mode.

II. STRUCTURE AND MECHANICAL STRENGTH OF PROPOSED HE-VFMM

A. STRUCTURE AND DESIGN PARAMETERS

Fig. 3 shows cross-sectional views of the proposed HE-VFMM and the target motor mounted in the Prius 4th generation. In this paper, the proposed HE-VFMM is compared to the target motor, which is an IPMSM with good performance for a better comparison to understand its effectiveness [10]. Both motors have the same stator structure and basic parameters such as dimensions, voltage, and rotational speed, as listed in Table 1. Heat generation in the winding is strongly related to the current density [11]. Accordingly, the armature current density of the proposed HE-VFMM was set to 27.5 Arms/mm² which is same as the target motor. On the other hand, since it is more difficult to cool the rotor than the stator, the maximum current density of the DC field current is 15 A/mm². The current value in this case is 12 A. Moreover, the magnetizing current pulse is three times the rated value because it is applied only for a short period of time. This means that the maximum magnetizing current pulse is 36 A. Additionally, the maximum value of demagnetization and magnetization currents is same each other.

Variable flux motors can be classified into several types depending on the variable flux scheme as shown in Fig. 2. Notably, many research groups have developed variable flux memory motors (VFMM) and hybrid excitation motors (HEM) [7], [12], [13], [14], [15]. VFMMs have variable-flux permanent magnets (VPM) that can change their magnetization ratio (MR) and magnetization direction (MD) by applying a current pulse. Accordingly, the VFMM can realize magnetic flux adjustment by changing the MR and MD of the

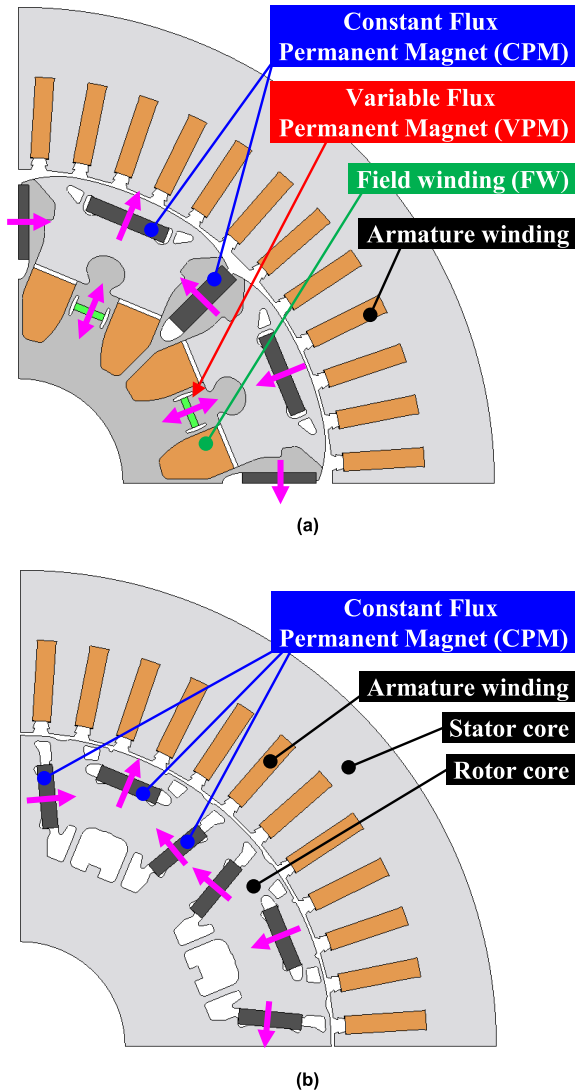


FIGURE 3. Cross-sectional Views of evaluated motors. (a) Proposed HE-VFMM. (b) Target motor mounted in Prius 4th generation for comparison.

VPM [16]. On the other hand, HEMs have both permanent magnets (PMs) and field windings, adjusting magnetic flux in the air gap by controlling the field current.

Table 2 lists comparison of VFMMs, HEMs, and the proposed HE-VFMM in traction applications. VFMMs have simple structure that is almost same as typical IPMSMs, realizing variable magnetic flux with low cost. On the other hand, VFMMs need to input magnetizing current pulse into the armature winding, and therefore, VPMs need to be installed close to the rotor surface. As a result, there is not much flexibility in the position of VPMs. This makes it easy to cause unintentional demagnetization, which is a critical issue in VFMMs because VPM is exposed to the diamagnetic field caused by load current in the armature winding, especially in traction applications. The unintentional demagnetization is an unexpected change in MR and MD of VPMs due to the armature current during operation or diamagnetic field caused by

TABLE 1. Main parameters and dimensions of proposed HE-VFMM.

Item	Value
Pole / Slot combination	8 pole / 48 slot*
Total axial length	118.5 mm*
Stator outer diameter	215 mm*
Max. DC-bus voltage	600 V*
Max. inverter current	180 Arms*
Max. armature current density	27.5 Arms/mm ² *
Max. rotational speed	17,000 rpm*
Rated field current density	15 A _{dc} /mm ² **
Max. magnetizing current density	45 A _{dc} /mm ² ***

(*Same value as target motor (Toyota Prius 4th generation))

(**Rated field current is 12 A (= 15 A_{dc}/mm²))

(***Maximum magnetizing current is 36 A (= 45 A_{dc}/mm²))

CPMs [17]. The unintentional demagnetization has been considered in several research groups. For example, double layer structure is effective in enhancing durability against the unintentional demagnetization of VPM [18]. However, the fact remains that there are restrictions on the location of the VPM in the VFMM.

HEMs have high controllability because a variable magnetic flux can be realized by simply changing the field current. Additionally, the PMs in HEMs are constant-flux permanent magnets (CPM) that have unchanged MR and MD. Therefore, the flexibility of the PM position in the HEMs is high. However, HEMs require additional field windings, leading to increased costs. Moreover, HEM can be classified according to whether the field winding is in the rotor or stator [19], [20]. HEMs with rotor winding require a slip ring, which causes maintenance and cost issues in traction applications [21]. However, in recent years, the problem has gradually improved, as seen in Renault’s ZOE, which uses a traction motor with a slip ring [22].

On the other hand, HEMs have critical issues in terms of efficiency in low-speed and middle-torque areas, which are frequently used [9]. The efficiency in that area is reduced by a constantly applied field current, which generates the field copper loss. Additionally, the copper loss in the field winding causes an increase in the rotor temperature. Therefore, the efficiency of conventional HEMs in this area is prone to decrease compared with that of typical IPMSMs.

Compared with the aforementioned conventional motors, the proposed HE-VFMM shown in Fig. 3(a) can overcome the issues of VFMMs and HEMs. Fig. 4 shows the principle of the variable flux scheme for each variable flux motor. As mentioned above, the VFMM shown in Fig. 4(a) realizes variable magnetic flux due to a change in the MR and MD of the VPMs. The magnetic flux of the HEM, shown in Fig. 4(b), is changed by adjusting the field current in the rotor. On the

TABLE 2. A Comparison of traction motors with different variable flux schemes.

Motor type	Components for variable magnetic flux	Advantages	Disadvantages
VFMM	VPM	<ul style="list-style-type: none"> • Simple structure (almost same as typical IPMSMs) • No additional components • Good manufacturability, low cost 	<ul style="list-style-type: none"> • Necessity of applying current pulse to armature winding • Low flexibility of PM position • Structure prone to unintentional demagnetization of VPM*
HEM	Field winding	<ul style="list-style-type: none"> • High controllability (Easy to change magnetic flux) • High flexibility of PM position 	<ul style="list-style-type: none"> • Higher cost due to additional field winding than VFMM • Low maintainability of slip ring • Low efficiency in low-speed operating area due to constantly generating field copper loss**
HE-VFMM (Proposed model)	VPM + Field winding	<ul style="list-style-type: none"> • Larger variable flux range than VFMM and HEM • High resistance to unintentional demagnetization of VPM (*Improving demerit of VFMM) • High efficiency by not applying field current steadily (**Improving demerit of HEM) • High efficiency over a wide operating area 	<ul style="list-style-type: none"> • Higher cost due to additional field winding than VFMM • Low maintainability of slip ring • Need to employ divided core

other hand, Fig. 4(c) shows the variable flux scheme of the proposed HE-VFMM. The proposed HE-VFMM combines the HEM with VFMM, having both the field winding and VPM. The proposed HE-VFMM achieves high performance while compensating for the drawbacks of the HEM and VFMM, as shown in Table 2. Unlike many conventional VFMMs, VPMs are installed on the inner side of the rotor in the proposed motor. Hence, the durability against unintentional demagnetization can be enhanced because the effect of the diamagnetic field from the armature current is restrained.

In Mode-1, a closed magnetic path in the rotor is constructed by some CPMs and VPMs after the VPM is demagnetized by magnetizing current applied to the field winding. As a result, the magnetic flux density in the air gap B_g is decreased, reducing the iron loss and induced voltage. In Mode-2, MD of VPM is reversed by current pulse applied to the field winding, and then B_g is increased. In contrast to the HEM, the proposed HE-VFMM does not require a constant input of the field current. This implies that the proposed HE-VFMM can improve the copper loss in the field winding of the HEM.

Furthermore, the proposed HE-VFMM can additionally enhance B_g by constantly applying a field current I_f under a certain condition, as shown in Mode-3. Accordingly, the proposed HE-VFMM realizes a larger variable flux range than conventional HEMs and VFMMs by seamlessly changing among the three modes.

In summary, the proposed VFMM uses two methods for adjusting the magnetic flux. The d -axis magnetic flux ψ_d of the proposed HE-VFMM can be defined as

$$\psi_d = L_d i_d + \psi_{cpm} + \psi_{vpm} + \psi_f \quad (1)$$

where L_d and i_d are the d -axis armature inductance and current, respectively; ψ_{cpm} and ψ_{vpm} are the flux linkages of the CPM and VPM, respectively; ψ_f is the magnetic flux generated by the field current I_f applied to the field winding on the rotor. Accordingly, the proposed HE-VFMM realizes a very large adjustable range of ψ_d owing to the adjustable ψ_{vpm} and ψ_f .

Additionally, the VPMs in the proposed HE-VFMM are remagnetized and demagnetized by a current pulse in the field winding. As a result, VPMs can be sufficiently magnetized, although they are installed on the inner side of the rotor. Furthermore, the proposed motor can prevent VPMs from unintentional demagnetization by applying a field current under heavy-load condition. This implies that the proposed HE-VFMM can improve the unintentional demagnetization problem of the VFMM.

B. ASSEMBLY PROCEDURE AND MECHANICAL STRENGTH, MATERIALS

The proposed HE-VFMM has two types of permanent magnet (PM) materials because a hybrid PM structure in the VFMM is employed [23]. The proposed HE-VFMM has NdFeB

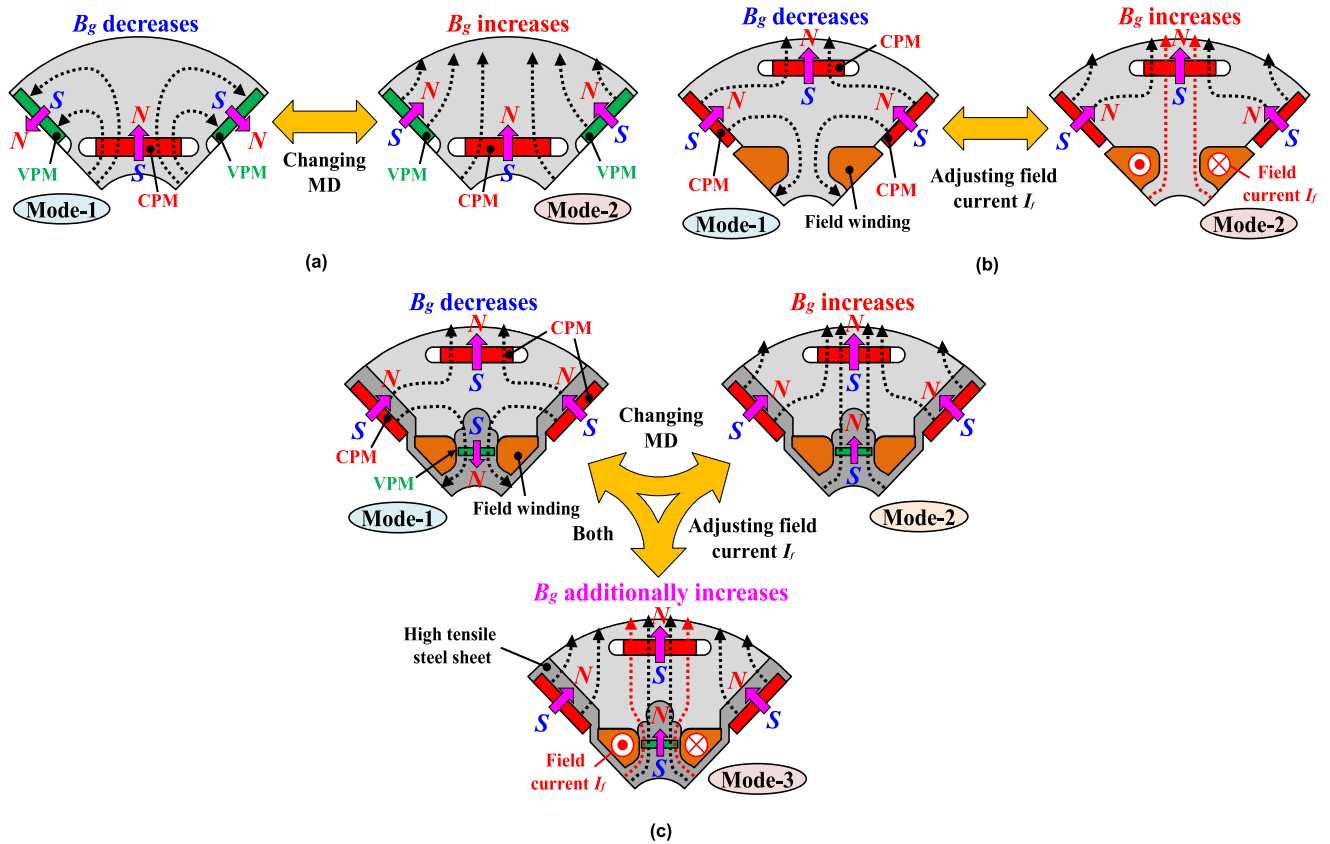


FIGURE 4. Principle of each variable flux scheme. (a) VFMM. (b) HEM. (c) Proposed HE-VFMM.

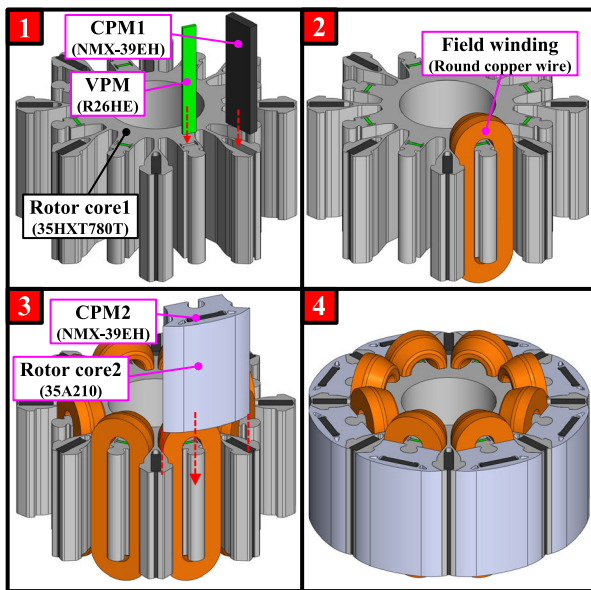


FIGURE 5. Assembly procedure of proposed rotor in HE-VFMM.

magnet (NMX-39EH, Hitachi Metal, Ltd.), which is a CPM and SmCo magnet (R26HE, Shin-Etsu Chemical, Co., Ltd.), which is a VPM.

Fig. 5 shows the assembly procedure for the proposed HE-VFMM. The proposed HE-VFMM has divided rotor cores,

because the field winding must be inserted inside the rotor. Firstly, VPM and CPM1, which are located between magnetic poles are inserted into rotor core1 that is a high-tensile steel sheet (35HXT780T, Nippon Steel Co., Ltd.). Secondly, the field winding is automatically wound on rotor core1 from outside. Thirdly, the CPM2 and the rotor core2 which is the electromagnetic steel sheet (35A210) are inserted into the rotor core1. As a result, the basic structure of the rotor is complete. The field current is supplied to the field winding in the rotor via a slip ring [24].

A structural analysis at the maximum rotational speed of 17,000 rpm is carried out to clarify the mechanical strength of the proposed HE-VFMM and the target motor (Prius). In this paper, the structural analysis did not consider the adhesive between the rotor core and PMs. Furthermore, the magnetic force was not considered in this analysis because the centrifugal force is dominant, especially in the high-speed region. The proposed HE-VFMM employs two types of materials in the rotor. In the area contributing to an increase in the reluctance torque uses the electromagnetic steel sheet (35A210) [25], and in other parts, the high-tensile steel sheet (35HXT780T) is used for enhancing mechanical strength of the rotor. The yield point strengths of the materials are 432 MPa and 860 MPa for the electromagnetic steel sheet and high-tensile steel sheet, respectively. Structural analysis was carried out using CAD software (SolidWorks) in this paper.

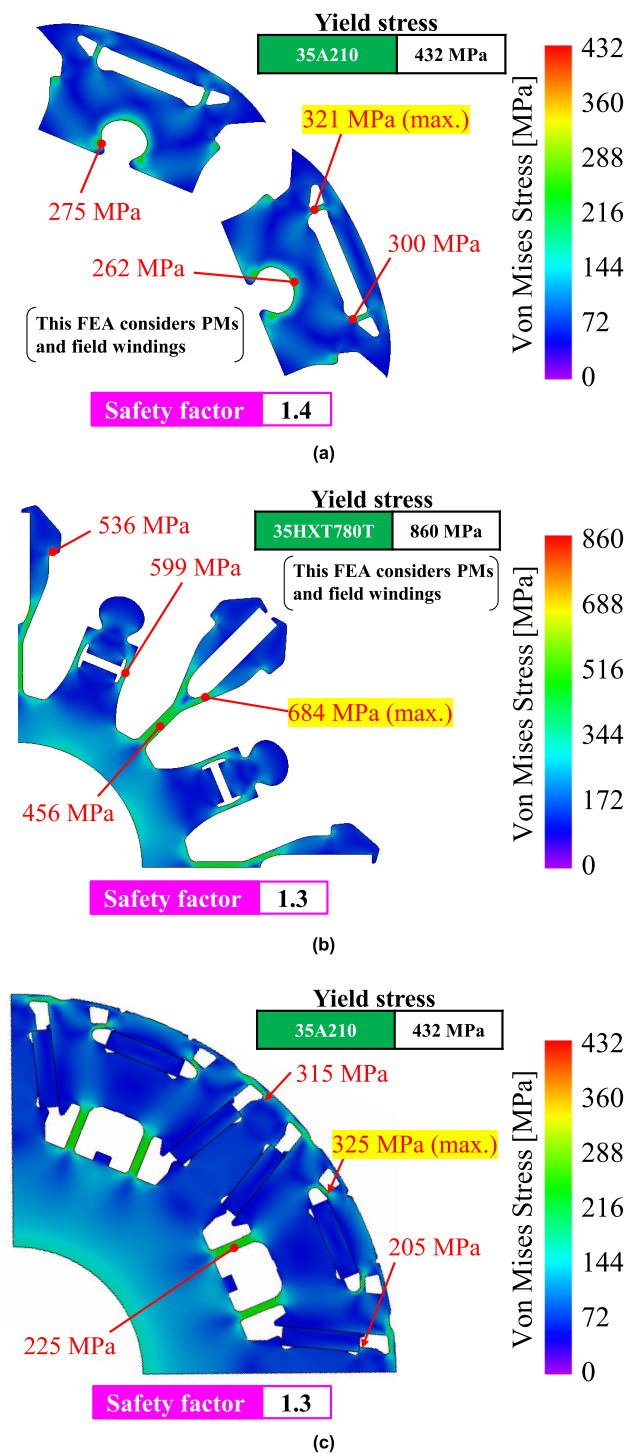


FIGURE 6. FEA predicted Von Mises Stress distributions at 17,000 rpm. (a) Electromagnetic steel sheet (35A210) in proposed HE-VFMM. (b) High tensile steel sheet (35HXT780T) in proposed HE-VFMM. (c) Target motor for comparison.

Fig. 6 shows the distribution of the von mises stress in the rotors of the two motors at 17,000 rpm. Fig. 6(a) shows the result of the electromagnetic steel sheet in the proposed HE-VFMM. The maximum von mises stress is 321 MPa at the

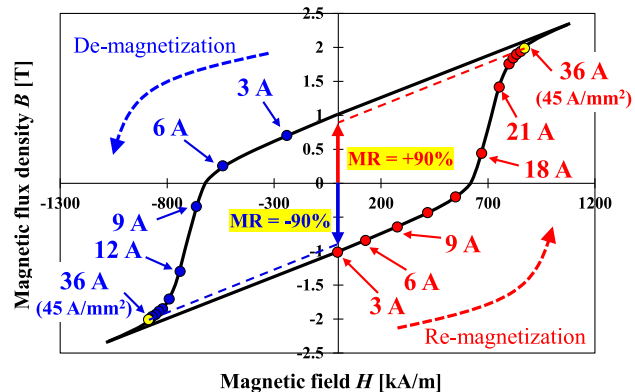


FIGURE 7. Operating point of VPMs when applying demagnetizing and re-magnetizing current pulse.

ribs located on both sides of the CPM, while the yield point strength is 432 MPa. Hence, the safety factor of the electromagnetic steel sheet is 1.4, and it was revealed that there is a sufficient margin of mechanical strength. Fig. 6(b) shows the distribution of the von mises stress of the high-tensile steel sheet. The maximum von mises stress is 684 MPa around the CPM located between poles, while the yield point strength is 860 MPa so that the safety factor of the high-tensile steel sheet is 1.3. Fig. 6(c) shows the von mises stress in the rotor of the target motor. The target motor has only an electromagnetic steel sheet (35A210). The maximum von mises stress is 325 MPa, getting a safety factor of 1.3. From the above, it was found that the proposed HE-VFMM with the divided rotor core can realize sufficient mechanical strength and feasibility because its safety factor is almost same as that of the commercially supplied motor mounted in Prius.

III. BASIC PERFORMANCE OF PROPOSED HE-VFMM

A. MAGNETIZATION CHARACTERISTIC

Fig. 7 shows operating point of VPMs when applying demagnetizing and re-magnetizing current pulse to the FW. As mentioned above, the maximum magnetizing current is 36 A. The MR of VPMs can be perfectly changed from +90% to -90% within maximum magnetizing current. Accordingly, the proposed HE-VFMM can realize variable magnetic flux by changing the MR. In addition, accuracy of the magnetization analysis is important. In our research group, magnetization characteristic simulated by 2D-FEA is in good agreement with the experimental results [24]. Other literature also reports that the error between experimental and FEA results in the magnetization characteristics of a VFMM is small [19].

B. VARIABLE FLUX PERFORMANCE UNDER NO-LOAD

Figs. 8 and 9 show the magnetic flux density distributions of the proposed HE-VFMM and the target motor under no-load condition, respectively. As shown in Fig. 8, the proposed HE-VFMM can dramatically change the magnetic flux density in the stator core because of the MR of the VPM and

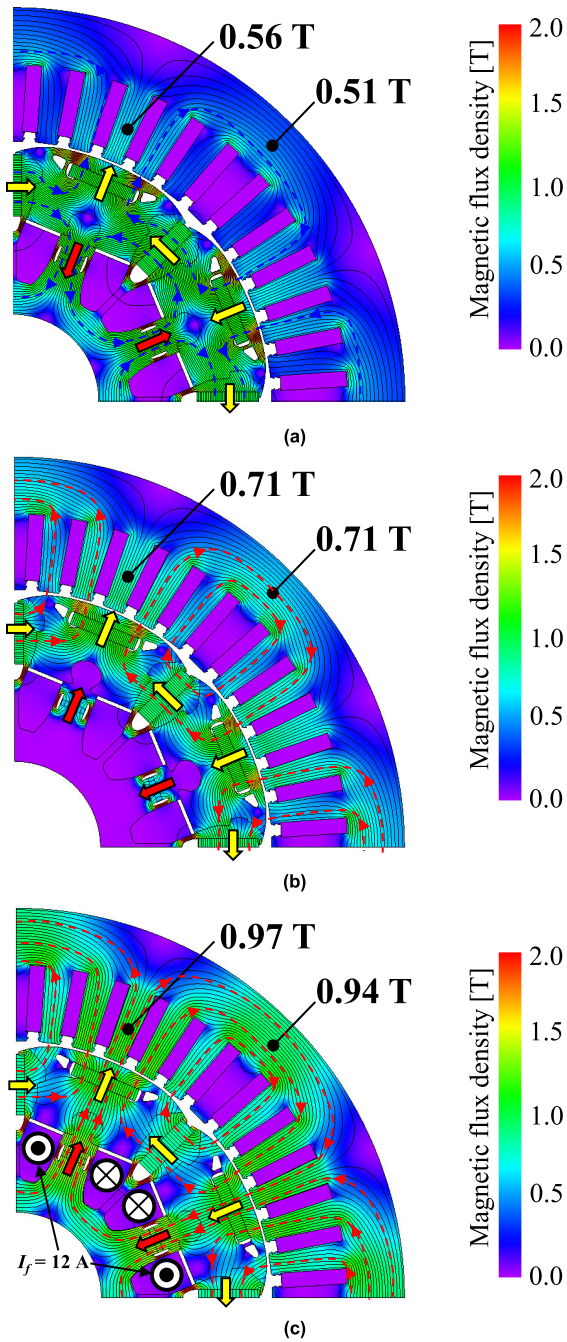


FIGURE 8. Magnetic flux density distributions at no-load condition. (a) Proposed HE-VFMM with MR = -90%, $I_f = 0$ A. (b) Proposed HE-VFMM with MR = +90%, $I_f = 0$ A. (c) Proposed HE-VFMM with MR = +90%, $I_f = 12$ A (15 A/mm²).

field current I_f . The magnetic flux density in the target motor is constant because it does not have a field winding or VPM. Additionally, the proposed HE-VFMM realizes lower and higher magnetic flux densities than the target motor simultaneously. This implies that the proposed HE-VFMM can simultaneously achieve high efficiency and high output power in high-speed areas.

Fig. 10 shows the air gap flux density waveforms of both motors under no-load condition. Fig. 10(a) indicates that the

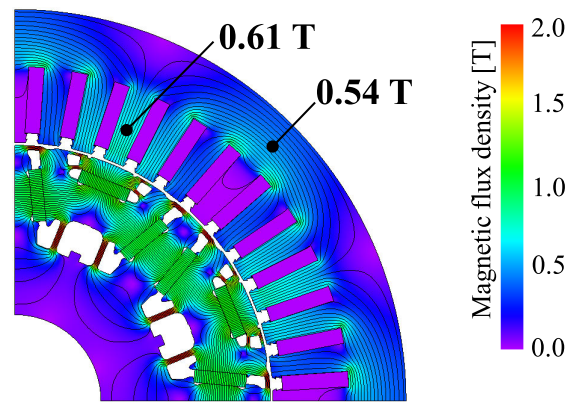


FIGURE 9. Magnetic flux density distributions of target motor (Prius) at no-load condition.

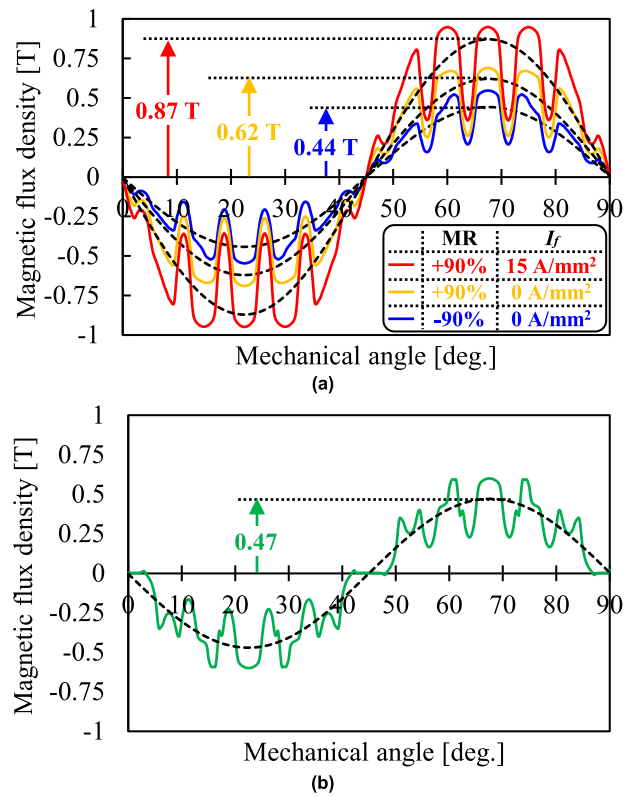


FIGURE 10. Air gap flux density waveforms under no-load condition. (a) Proposed HE-VFMM in different MR conditions. (b) Target motor.

proposed HE-VFMM can dramatically change the magnetic flux in the air gap. In case that an MR is -90% and I_f is 0 A, fundamental amplitude of the magnetic flux waveforms is 0.44 T in the proposed HE-VFMM. This value is lower than that of the target motor shown in Fig. 10(c). On the other hand, the proposed VFMM with an MR of +90% and I_f of 15 A/mm² achieves 85% higher amplitude compared to the target motor. It can be predicted that the proposed HE-VFMM is able to realize higher output power than that of the target motor.

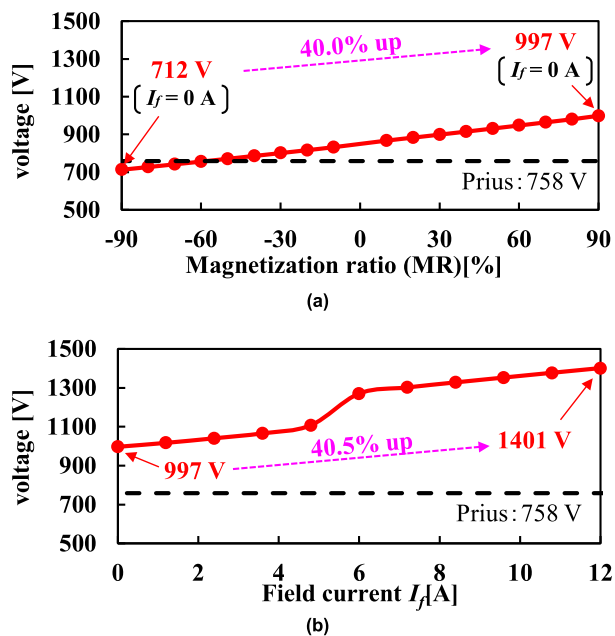


FIGURE 11. No-load voltage of both motors at maximum rotational speed of 17,000 rpm. (a) Case of MR changes. (b) Case of the field current changes.

Fig. 11 shows the no-load line-to-line voltage of the proposed HE-VFMM and the target motor at 17,000 rpm when the MR of the VPM and field current I_f are changed. The proposed HE-VFMM with an MR of -90% has almost the same value as that of the target motor. On the other hand, with an MR of +90%, the induced voltage is increased by 40.0%, as shown in Fig. 11(a). The proposed motor can additionally enhance the magnetic flux density in the air gap by applying a field current I_f , and therefore, the induced voltage increases by 40.5%, as shown in Fig. 11(b). In summary, the proposed motor has the capability of enhancing the output power under the six-step operation mode in a high-speed area by adjustable magnetic flux due to VPM and field current.

The iron loss of the proposed HE-VFMM also varies with the MR of the VPM and field current, similar to the induced voltage. Fig. 12 shows the no-load iron loss of the proposed HE-VFMM and target motor at 17,000 rpm when the MR of VPM and the field current I_f are changed. The proposed HE-VFMM with an MR of -90% has 24.6% lower iron loss than that of the target motor. Hence it can be predicted that the proposed HE-VFMM realizes higher efficiency in the operating region where the iron loss is dominant.

Notably, in Figs. 11(b) and 12(b), there is a sudden change in the voltage and iron loss when the field current switch from 4.8 A to 6 A. This is because the direction of the magnetic flux flow on both sides of the VPM is reversed by the field current, as shown in Fig. 13.

C. MAXIMUM TORQUE PERFORMANCE AT LOW-SPEED

Fig. 14 shows the magnetic flux density distributions of the proposed HE-VFMM and target motor at 3000 rpm and a

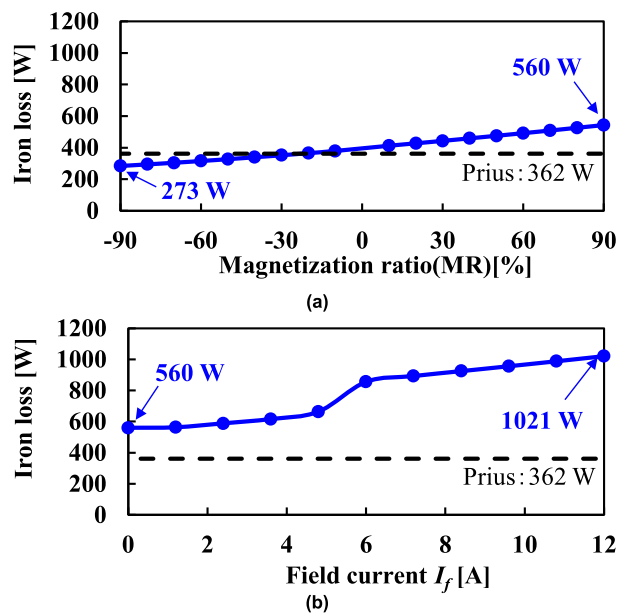


FIGURE 12. No-load iron loss of both motors at maximum rotational speed of 17,000 rpm. (a) Case of MR changes. (b) Case of the field current changes.

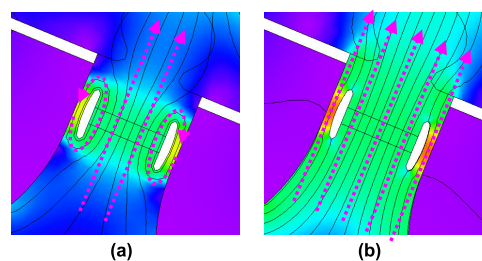


FIGURE 13. Magnetic flux density and magnetic flux flows when field current is changed under no-load condition. (a) $I_f = 4.8$ A. (b) $I_f = 6$ A.

maximum armature current of 180 Arms. The current phase angles are 50 deg. and 55 deg., respectively. Fig. 15 shows the corresponding torque waveforms for both motors. The stator cores of both motors are markedly saturated by the large armature current. To increase the magnetic flux of the proposed HE-VFMM, the MR of the VPM and the field current are set to maximum values of +90% and 12 A, respectively. However, the average torques of the two motors are almost the same, although the no-load voltage has a very large difference, as described in Fig. 11. This is due to the magnetic saturation in the stator core at this operating point, which requires the maximum torque. On the other hand, it can also be described that the proposed HE-VFMM achieves the same high torque density as the target motor.

IV. OUTPUT POWER PERFORMANCE IN SIX-STEP OPERATION MODE

In this section, the output power and efficiency of the proposed HE-VFMM and target motor are compared in the six-step operation mode. Additionally, a suitable rotor shape

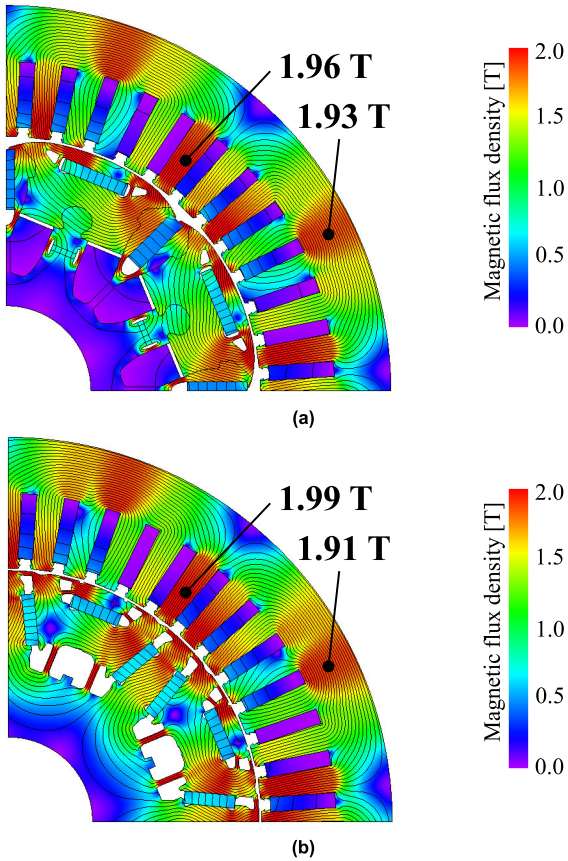


FIGURE 14. Magnetic flux density distributions under maximum torque condition at 3000 rpm and 180 Arms. (a) Proposed HE-VFMM (MR = +90%, $I_f = 12$ A). (b) Target motor mounted in Prius.

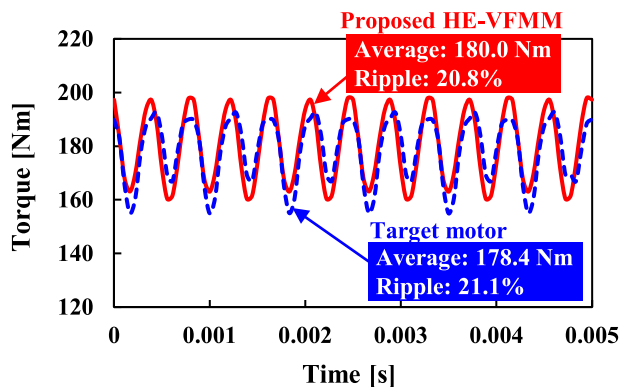


FIGURE 15. Torque waveforms of both motors under maximum torque condition at 3000 rpm and 180 Arms.

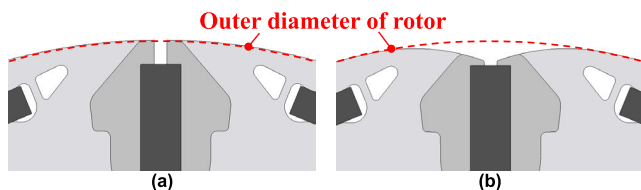


FIGURE 16. Modification of rotor shape in HE-VFMM to reduce iron loss in six-step operation mode. (a) Conventional model. (b) Proposed model with non-constant air gap.

of the HE-VFMM for enhancing the efficiency of the six-step operation is also described. The current waveforms (see Fig. 20) and magnetic properties of both motors are calculated

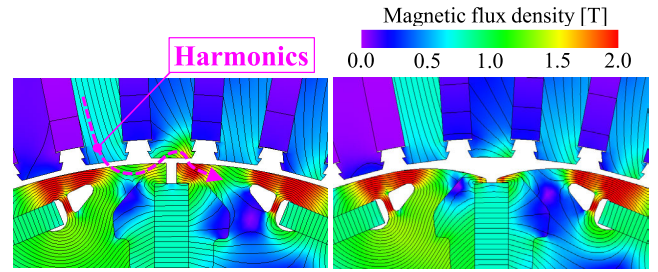


FIGURE 17. Magnetic flux density distributions in two HE-VFMMs in six-step operation mode (17000 rpm, 24 Nm). (a) Conventional model (MR = +90%). (b) Proposed model with non-constant air gap (MR = +10%).

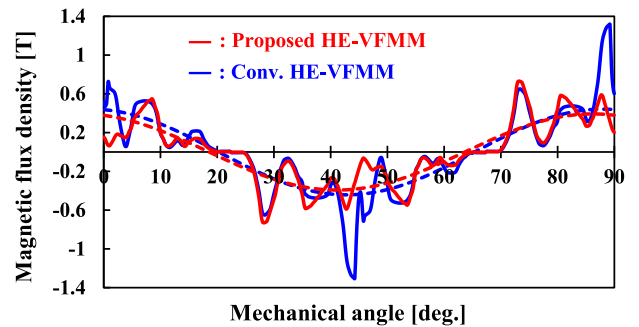


FIGURE 18. Air gap flux density waveforms of two HE-VFMM in six-step operation mode (17000 rpm, 24 Nm).

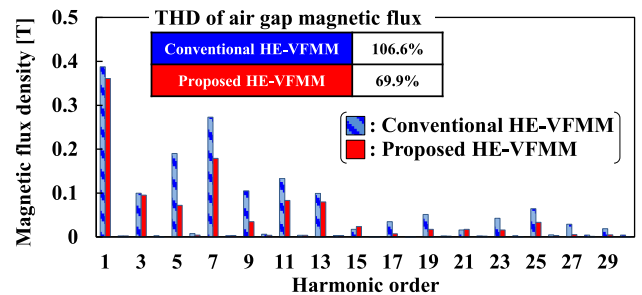


FIGURE 19. Harmonic spectrum of magnetic flux density in the air gap of two HE-VFMMs in six-step operation mode (17000 rpm, 24 Nm).

using an electromagnetic field simulator (JMAG-designer, ver. 21.0, JSOL Co., Ltd.).

A. SUITABLE ROTOR STRUCTURE FOR ENHANCING EFFICIENCY IN SIX-STEP OPERATION MODE

Fig. 16 shows the two rotor shapes of the HE-VFMM. The rotor shape shown in Fig. 16(a) has a typical constant-air-gap structure. In contrast, the proposed rotor structure shown in Fig. 16(b) employs a non-constant air gap. A non-constant air gap can reduce the harmonic components of the magnetic flux in the air gap, and therefore, the iron loss can be reduced. Fig. 17 shows the magnetic flux density distributions of the two HE-VFMMs employing different rotor shapes in the six-step operation mode at 17,000 rpm and 24 Nm. Harmonic magnetic flux occurs in the air gap of the conventional model, as shown in Fig. 17(a). On the other hand, the harmonic

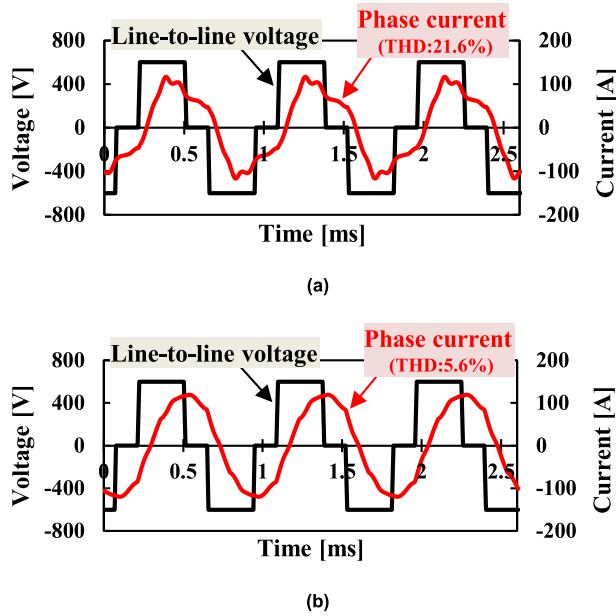


FIGURE 20. Voltage and calculated current waveform of two HE-VFMMs in six-step operation mode (17,000 rpm, $V_{dc} = 600$ V). (a) Conventional HE-VFMM employing constant air gap (MR = +90%, $I_f = 0$ A). (b) Proposed HE-VFMM employing non-constant air gap (MR = +10%, $I_f = 0$ A).

flux obviously decreases in the proposed model, as shown in Fig. 17(b), owing to the proposed non-constant air gap.

Fig. 18 shows Air gap flux density waveforms of two HE-VFMM in six-step operation mode (17000 rpm, 24 Nm).

Fig. 19 shows the harmonic spectrum of the magnetic flux density in the air gap of the two HE-VFMMs in the six-step operation mode at 17,000 rpm, 24 Nm. The total harmonic distortion (THD) of the magnetic flux density in the air gap of the conventional and proposed HE-VFMM are 106.6% and 69.9%, respectively. This means that the proposed non-constant air gap is highly effective in reducing the THD of the magnetic flux in the air gap.

Fig. 20 shows the voltage and current waveforms in the conventional and proposed HE-VFMMs under six-step operation at a maximum rotational speed and DC-bus voltage of 600 V. Because of the six-step operation, the current waveforms include harmonics [26]. The applied current waveform of the conventional HE-VFMM using a constant air gap has a large THD of 21.6% because of the large harmonics of the magnetic flux in the air gap. On the other hand, the proposed HE-VFMM using a non-constant air gap can reduce the THD of the current waveform to 5.6%, as shown in Fig. 20(b). As a result, the applied current of the proposed HE-VFMM is close to a sine wave, which contributes to reducing iron loss.

Fig. 21 shows the loss and efficiency of the two HE-VFMMs and the target motor mounted in Prius 4th generation at the same operating point in the six-step operation mode. The conventional HE-VFMM with a constant air gap has the largest iron loss owing to the harmonics of the magnetic flux and input current. Consequently, the efficiency

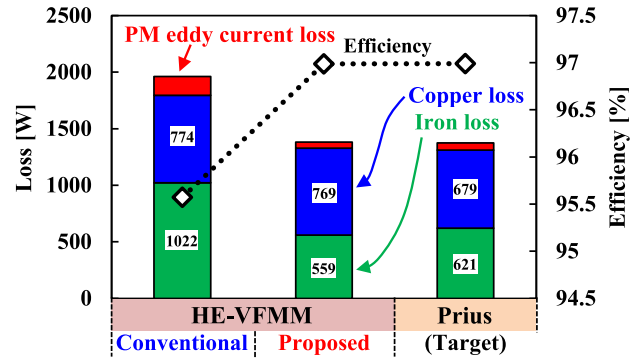


FIGURE 21. Loss and efficiency of conventional HE-VFMM (MR = +90%, $I_f = 0$ A) and proposed HE-VFMM with non-constant air gap (MR = +10%, $I_f = 0$ A) and target motor (Prius) in six-step operation (17,000 rpm, 24 Nm).

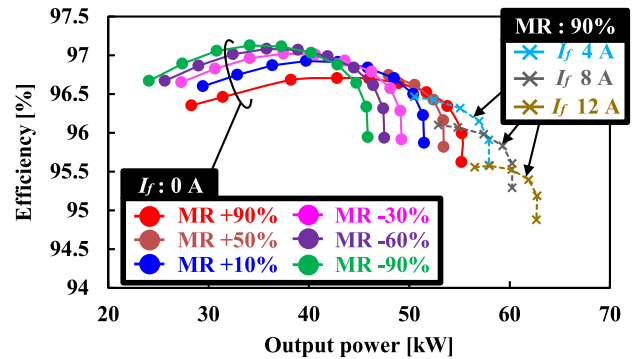


FIGURE 22. Efficiency and output power of proposed HE-VFMM when MR of VPM and I_f are changed in six-step operation mode (17,000 rpm, 600 V).

is the lowest. On the other hand, the proposed HE-VFMM employing a non-constant air gap realizes the same efficiency as the target motor at an operating point of 43 kW because the harmonics of the magnetic flux and input current can be reduced.

B. OUTPUT POWER CHARACTERISTIC IN SIX-STEP OPERATION MODE

Fig. 22 shows the efficiency versus output power of the proposed HE-VFMM when the MR of the VPM and field current I_f are changed in the six-step operation mode at 17,000 rpm. As the MR and field current increase, the output power can be significantly improved by increasing d -axis magnetic flux ψ_d . As a result, the proposed HE-VFMM can achieve 23.7% higher output power than that of the target motor as shown in Fig. 23 while maintaining almost the same efficiency in the low-power area as the target motor.

Fig. 24 shows the torque increasing ratio k versus the MR and I_f of the proposed HE-VFMM at two operating points. The torque increasing ratio k is defined as

$$k = \frac{T_k - T_{base}}{T_{base}} \times 100 \quad (2)$$

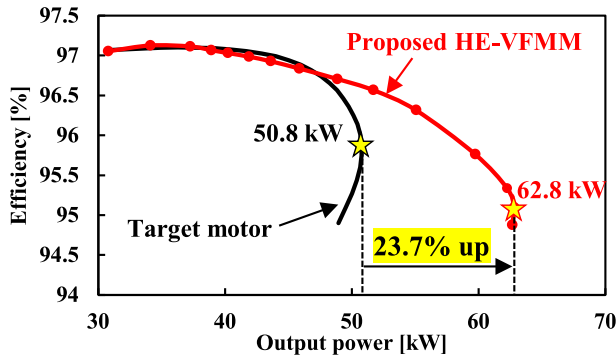


FIGURE 23. Comparison of efficiency and output power between proposed HE-VFMM and target motor in six-step operation mode (17,000 rpm, 600 V).

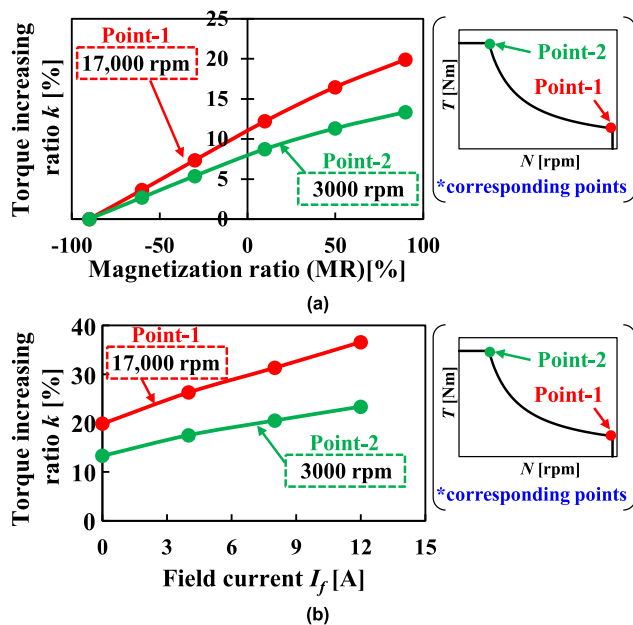


FIGURE 24. Torque increasing ratio k of proposed HE-VFMM when generating maximum torque at each operating point. (a) Case of MR changes. (b) Case of the field current changes.

where T_{base} is the torque of the proposed HE-VFMM when MR is -90% and I_f is 0 A, respectively (namely, the smallest torque); T_k is the torque when MR and the field current are changed. At Point-1, k is evaluated in six-step operation mode at 17,000 rpm. Point-2 is set to 3,000 rpm and 180 Arms. In Fig. 24, k at Point-1 is higher than at Point-2 because the magnetic saturation in the stator core is mitigated at Point-1 due to smaller armature current and the field weakening control, as shown in Figs. 14 and 17, respectively. This result indicates that the variable flux function is more effective at higher rotational speeds.

Fig. 25 shows the output power of the proposed HE-VFMM and target motor as functions of the rotational speed. The proposed HE-VFMM realizes a much higher output power than the target motor because of the variable flux functions. Additionally, as the rotational speed increases,

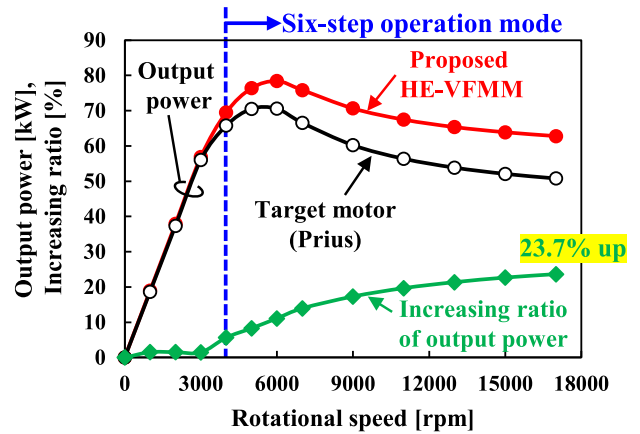


FIGURE 25. Output power of both motors and an increasing ratio of output power of proposed HE-VFMM compared with target motor over a wide operating area ($V_{dc} = 600$ V).

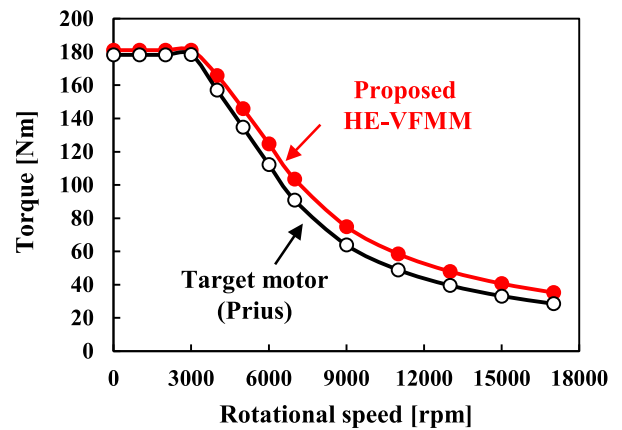


FIGURE 26. N-T curves of proposed HE-VFMM and target motor ($V_{dc} = 600$ V).

an increasing ratio of the output power becomes higher. This is because the torque increasing ratio k is higher, especially in the high-speed area. Furthermore, Fig. 26 indicates N-T characteristics of the proposed VFMM and target motor. The proposed HE-VFMM achieves higher torque, especially in high-speed area.

V. CONCLUSION

This paper proposed a novel HE-VFMM that achieves an adjustable magnetic flux over a wide range and assessed how it performs in a high-speed area with a six-step operation mode. In addition to the higher torque and efficiency than those of the target motor mounted in Toyota Prius 4th generation, the proposed HE-VFMM realizes 23.7% higher output power at 17,000 rpm in the six-step operation while maintaining the same motor size. Additionally, this paper shows a suitable rotor shape to enhance the efficiency of the HE-VFMM in a six-step operation. Moreover, it was found that the variable flux functions were more effective in increasing the output power, especially in high-speed areas. Consequently, the proposed HE-VFMM simultaneously realizes

(i) high efficiency over a wide operating area, (ii) high torque performance in low-speed areas, and (iii) high output power characteristics in high-speed areas. In summary, the proposed HE-VFMM is a good candidate for EV/HEV traction.

REFERENCES

- [1] F. Momen, K. Rahman, and Y. Son, "Electrical propulsion system design of Chevrolet bolt battery electric vehicle," *IEEE Trans. Ind. Appl.*, vol. 55, no. 1, pp. 376–384, Jan. 2019, doi: [10.1109/TIA.2018.2868280](https://doi.org/10.1109/TIA.2018.2868280).
- [2] T. Zou, D. Gerada, S. La Rocca, A. La Rocca, A. Walker, G. Vakil, S. L. Arevalo, Z. Xu, M. Cui, A. Bardalai, and M. Wang, "Airgap length analysis of a 350 kw PM-assisted syn-rel machine for heavy duty EV traction," *IEEE Trans. Ind. Appl.*, vol. 59, no. 2, pp. 1557–1570, Mar. 2023, doi: [10.1109/TIA.2022.3225255](https://doi.org/10.1109/TIA.2022.3225255).
- [3] G. Pellegrino, A. Vagati, B. Boazzo, and P. Guglielmi, "Comparison of induction and PM synchronous motor drives for EV application including design examples," *IEEE Trans. Ind. Appl.*, vol. 48, no. 6, pp. 2322–2332, Nov. 2012, doi: [10.1109/TIA.2012.2227092](https://doi.org/10.1109/TIA.2012.2227092).
- [4] C. Yu and K. T. Chau, "Design, analysis, and control of DC-excited memory motors," *IEEE Trans. Energy Convers.*, vol. 26, no. 2, pp. 479–489, Jun. 2011, doi: [10.1109/TEC.2010.2085048](https://doi.org/10.1109/TEC.2010.2085048).
- [5] M. Ibrahim, L. Masisi, and P. Pillay, "Design of variable-flux permanent-magnet machines using alnico magnets," *IEEE Trans. Ind. Appl.*, vol. 51, no. 6, pp. 4482–4491, Nov. 2015, doi: [10.1109/TIA.2015.2461621](https://doi.org/10.1109/TIA.2015.2461621).
- [6] N. Limsuwan, T. Kato, K. Akatsu, and R. D. Lorenz, "Design and evaluation of a variable-flux flux-intensifying interior permanent-magnet machine," *IEEE Trans. Ind. Appl.*, vol. 50, no. 2, pp. 1015–1024, Mar. 2014, doi: [10.1109/TIA.2013.2273482](https://doi.org/10.1109/TIA.2013.2273482).
- [7] Y. Yan, Y. Fan, F. Shen, H. Chen, S. Cai, X. Yuan, and C. H. T. Lee, "Hybrid-magnet variable flux memory machine with improved field regulation capability for electric vehicle applications," *IEEE Trans. Transport. Electric.*, vol. 9, no. 1, pp. 586–597, Mar. 2023, doi: [10.1109/TTE.2022.3188868](https://doi.org/10.1109/TTE.2022.3188868).
- [8] D. Michieletto, L. Cinti, and N. Bianchi, "Hybrid excitation PM synchronous motors: Part I—Per unit analysis," *IEEE Trans. Energy Convers.*, vol. 37, no. 1, pp. 487–494, Mar. 2022, doi: [10.1109/TEC.2021.3107937](https://doi.org/10.1109/TEC.2021.3107937).
- [9] K. Yokomichi, R. Tsunata, M. Takemoto, and J. Imai, "A proposal of hybrid excitation variable flux memory motor having field winding with magnetization function in the rotor," in *Proc. IEEE Energy Convers. Congr. Expo. (ECCE)*, Oct. 2022, pp. 1–8, doi: [10.1109/ECCE50734.2022.9947959](https://doi.org/10.1109/ECCE50734.2022.9947959).
- [10] K. Haruno, "Development of new motor for compact class hybrid vehicles," in *Proc. Soc. Automot. Engineers Jpn. (JSAE) Spring Conf.*, May 2016, pp. 1095–1099.
- [11] R. Tsunata, M. Takemoto, J. Imai, T. Saito, and T. Ueno, "Comparison of thermal characteristics in various aspect ratios for radial-flux and axial-flux permanent magnet machines," *IEEE Trans. Ind. Appl.*, vol. 59, no. 3, pp. 3353–3367, May/Jun. 2023, doi: [10.1109/TIA.2023.3255845](https://doi.org/10.1109/TIA.2023.3255845).
- [12] Y. Xie, Z. Ning, and Z. Ma, "Comparative study on variable flux memory machines with different arrangements of permanent magnets," *IEEE Access*, vol. 8, pp. 164304–164312, 2020, doi: [10.1109/ACCESS.2020.3022595](https://doi.org/10.1109/ACCESS.2020.3022595).
- [13] H. Hua, Z. Q. Zhu, A. Pride, R. P. Deodhar, and T. Sasaki, "A novel variable flux memory machine with series hybrid magnets," *IEEE Trans. Ind. Appl.*, vol. 53, no. 5, pp. 4396–4405, Sep. 2017, doi: [10.1109/TIA.2017.2709261](https://doi.org/10.1109/TIA.2017.2709261).
- [14] L. Cinti, D. Michieletto, N. Bianchi, and M. Bertoluzzo, "A comparison between hybrid excitation and interior permanent magnet motors," in *Proc. IEEE Workshop Electr. Mach. Design, Control Diagnosis (WEMDCD)*, Apr. 2021, pp. 10–15, doi: [10.1109/WEMDCD51469.2021.9425634](https://doi.org/10.1109/WEMDCD51469.2021.9425634).
- [15] L. Zhang, Y. Fan, R. D. Lorenz, R. Cui, C. Li, and M. Cheng, "Design and analysis of a new five-phase brushless hybrid-excitation fault-tolerant motor for electric vehicles," *IEEE Trans. Ind. Appl.*, vol. 53, no. 4, pp. 3428–3437, Jul. 2017, doi: [10.1109/TIA.2017.2685359](https://doi.org/10.1109/TIA.2017.2685359).
- [16] V. Ostovic, "Memory motors—A new class of controllable flux PM machines for a true wide speed operation," in *Proc. Conf. Rec. IEEE Ind. Appl. Conf., 36th IAS Annu. Meeting*, Oct. 2001, pp. 2577–2584, doi: [10.1109/IAS.2001.955983](https://doi.org/10.1109/IAS.2001.955983).
- [17] D. Wu, Z. Q. Zhu, X. Liu, A. Pride, R. Deodhar, and T. Sasaki, "Cross coupling effect in hybrid magnet memory motor," in *Proc. 7th IET Int. Conf. Power Electron., Mach. Drives (PEMD)*, Manchester, U.K., Apr. 2014, pp. 1–6, doi: [10.1049/cp.2014.0319](https://doi.org/10.1049/cp.2014.0319).
- [18] R. Tsunata, M. Takemoto, S. Ogasawara, and K. Orikawa, "Variable flux memory motor employing double-layer delta-type PM arrangement and large flux barrier for traction applications," *IEEE Trans. Ind. Appl.*, vol. 57, no. 4, pp. 3545–3561, Jul. 2021, doi: [10.1109/TIA.2021.3068329](https://doi.org/10.1109/TIA.2021.3068329).
- [19] R. Nakazawa, M. Takemoto, S. Ogasawara, R. Tsunata, and K. Orikawa, "Examination of the characteristics of a hybrid excitation motor with field winding on a rotor for electric vehicle and hybrid vehicle traction," in *Proc. 48th Annu. Conf. IEEE Ind. Electron. Soc.*, Brussels, Belgium, Oct. 2022, pp. 1–6, doi: [10.1109/IECON49645.2022.9968604](https://doi.org/10.1109/IECON49645.2022.9968604).
- [20] S. Wu, Y. Wang, and W. Tong, "Design and analysis of new modular stator hybrid excitation synchronous motor," *CES Trans. Electr. Mach. Syst.*, vol. 6, no. 2, pp. 188–194, Jun. 2022, doi: [10.30941/CESTEMS.2022.00025](https://doi.org/10.30941/CESTEMS.2022.00025).
- [21] F. Zhang, G. Jia, Y. Zhao, Z. Yang, W. Cao, and J. L. Kirtley, "Simulation and experimental analysis of a brushless electrically excited synchronous machine with a hybrid rotor," *IEEE Trans. Magn.*, vol. 51, no. 12, pp. 1–7, Dec. 2015, doi: [10.1109/TMAG.2015.2450684](https://doi.org/10.1109/TMAG.2015.2450684).
- [22] (Sep. 2019). *Compare ZOE*. [Online]. Available: <https://www.renault.co.uk/vehicles/new-vehicles/zoe/compare.html>
- [23] H. Yang, R. Tu, H. Lin, S. Niu, and S. Lyu, "Investigation of balanced bidirectional-magnetization effect of a novel hybrid-magnet-circuit variable-flux memory machine," *IEEE Trans. Magn.*, vol. 58, no. 2, pp. 1–6, Feb. 2022, doi: [10.1109/TMAG.2021.3085750](https://doi.org/10.1109/TMAG.2021.3085750).
- [24] R. D. Hall and R. P. Roberge, "Carbon brush performance on slip rings," in *Proc. Conf. Rec. Annu. Pulp Paper Ind. Tech. Conf.*, Jun. 2010, pp. 1–6.
- [25] R. Tsunata, M. Takemoto, S. Ogasawara, and K. Orikawa, "Investigation of enhancing reluctance torque of a delta-type variable flux memory motor having large flux barrier for EV/HEV traction," in *Proc. IEEE Energy Convers. Congr. Expo. (ECCE)*, Oct. 2020, pp. 53–60, doi: [10.1109/ECCE44975.2020.9235600](https://doi.org/10.1109/ECCE44975.2020.9235600).
- [26] X. Fang, S. Lin, X. Wang, Z. Yang, F. Lin, and Z. Tian, "Model predictive current control of traction permanent magnet synchronous motors in six-step operation for railway application," *IEEE Trans. Ind. Electron.*, vol. 69, no. 9, pp. 8751–8759, Sep. 2022, doi: [10.1109/TIE.2021.3114695](https://doi.org/10.1109/TIE.2021.3114695).



REN TSUNATA (Member, IEEE) was born in Miyagi, Japan, in 1992. He received the B.S., M.S., and Ph.D. degrees in electrical engineering from Hokkaido University, Hokkaido, Japan, in 2015, 2017, and 2021, respectively.

From 2017 to 2018, he was with Toyota Motor Corporation, Aichi, Japan. In 2021, he joined Okayama University Okayama, Japan, as a Research Fellow, where he has been an Assistant Professor with the Graduate School of Natural Science and Technology, since 2022. His research interests include permanent magnet synchronous machines, variable flux motors, and axial flux machines. He is a member of the Institute of Electrical Engineers of Japan (IEEJ) and the Japan Society of Applied Electromagnetics and Machines (JSAEM). He was a recipient of four IEEJ Excellent Presentation Awards in 2017, 2020, and 2022, and the Incentive Award from JSAEM, in 2020.



KEITO YOKOMICHI was born in Shiga, Japan, in 1999. He received the B.S. degree in electrical engineering from the Department of Electrical and Communication Engineering, Okayama University, Japan, in 2021, and the M.S. degree in electrical engineering from the Graduate School of Natural Science and Technology, Okayama University, in 2023. He is a member of the Institute of Electrical Engineers of Japan (IEEJ).



MASATSUGU TAKEMOTO (Member, IEEE) was born in Tokyo, Japan, in 1972. He received the B.S. and M.S. degrees in electrical engineering from the Tokyo University of Science, Noda, Japan, in 1997 and 1999, respectively, and the Ph.D. degree in electrical engineering from the Tokyo Institute of Technology, Tokyo, in 2005.

In 1999, he joined the Department of Electrical Engineering, Tokyo Institute of Technology, as a Research Associate. In 2004, he joined the Department of Mechanical Systems Engineering, Musashi Institute of Technology, Tokyo, as a Research Associate, where he became a Lecturer, in 2005. In 2008, he joined the Graduate School of Information Science and Technology, Hokkaido University, Sapporo, as an Associate Professor. Since 2020, he has been with Okayama University, Okayama, Japan, where he is currently a Professor with the Graduate School of Natural Science and Technology. He is engaged in research on permanent magnet synchronous motors, axial gap motors, rare-earth-free motors, bearingless motors, and magnetic bearings. He is a member of the Institute of Electrical Engineers of Japan (IEEJ). He was a recipient of the Nagamori Award from the Nagamori Foundation, in 2017, the IEEJ Transaction Paper Award, in 2005, the Prize Paper Awards from the Electric Machines Committee of the IEEE Industry Applications Society, in 2011 and 2019, and the Prize Paper Award from the Electrical Machines Technical Committee of the IEEE Industrial Electronics Society, in 2018. He has served as a Secretary, the Vice-Chair, and the Chair for the IEEE IAS Japan Chapter, in 2008–2009, 2010–2011, and 2012–2013, respectively.



JUN IMAI (Member, IEEE) was born in Okayama, Japan, in 1964. He received the B.S., M.S., and Ph.D. degrees in electrical engineering from the Department of Electrical Engineering, Kyushu University, in 1987, 1989, and 1992, respectively. In 2000, he became a Lecturer with Okayama University, where he has been an Associate Professor, since 2008. His research interest includes modeling and control of distributed parameter systems, especially in performance limitation issues of physical control systems.

• • •